Molecular Therapy
Methods & Clinical Development
Original Article

Gene replacement therapy in a schwannoma mouse model of neurofibromatosis type 2

Shilpa Prabhakar,[1,15] Roberta L. Beauchamp,[2,15] Pike See Cheah,[3,4] Akiko Yoshinaga,[5,16] Edwina Abou Haidar,[1,16] Sevda Lule,[5] Gayathri Mani,[5] Katia Maalouf,[1] Anat Stemmer-Rachamimov,[6] David H. Jung,[7,9] D. Bradley Welling,[8,9] Marco Giovannini,[10] Scott R. Plotkin,[11] Casey A. Maguire,[12] Vijaya Ramesh,[13] and Xandra O. Breakefield[14]

[1]Department of Neurology and Center for Molecular Imaging Research, Massachusetts General Hospital, Harvard Medical School, Boston, MA 02114, USA; [2]Center for Genomic Medicine, Massachusetts General Hospital, Boston, MA 02114, USA; [3]Department of Neurology, Massachusetts General Hospital and Harvard Medical School, Center for Molecular Imaging Research, Massachusetts General Hospital, 25 Shattuck St, Boston, MA 02115, USA; [4]Department of Human Anatomy, Faculty of Medicine and Health Sciences, Universiti Putra Malaysia, JALAN UNIVERSITI 1 Serdang, 43400 Seri Kembangan, Selangor, Malaysia; [5]Department of Neurology and Center for Molecular Imaging Research, Massachusetts General Hospital and Harvard Medical School, Boston, MA 02129, USA; [6]Department of Pathology and Center for Cancer Research, Massachusetts General Hospital and Harvard Medical School, Boston, MA 02114, USA; [7]Department of Otolaryngology, Massachusetts Eye and Ear and Harvard Medical School, Boston, MA 02114, USA; [8]Department of Otolaryngology Head and Neck Surgery, Harvard Medical School, Massachusetts Eye and Ear and Massachusetts General Hospital, Boston, MA 02114, USA; [9]Program in Speech and Hearing Bioscience and Technology, Harvard Medical School, Boston, MA 02114, USA; [10]Department of Head and Neck Surgery, David Geffen School of Medicine at UCLA and Jonsson Comprehensive Cancer Center (JCCC), University of California Los Angeles, Los Angeles, CA 90095, USA; [11]Department of Neurology and Cancer Center, Massachusetts General Hospital and Harvard Medical School, Boston, MA 02114, USA; [12]Department of Neurology, Massachusetts General Hospital and NeuroDiscovery Center, Harvard Medical School, Boston, MA 02114, USA; [13]Department of Neurology and Center for Genomic Medicine, Massachusetts General Hospital and Harvard Medical School, Boston, MA 02114, USA; [14]Department of Neurology and Center for Molecular Imaging Research, Department of Radiology, Massachusetts General Hospital and Harvard Medical School, Boston, MA 02114, USA

Loss of function of the neurofibromatosis type 2 (NF2) tumor suppressor gene leads to the formation of schwannomas, meningiomas, and ependymomas, comprising ~50% of all sporadic cases of primary nervous system tumors. NF2 syndrome is an autosomal dominant condition, with bi-allelic inactivation of germline and somatic alleles resulting in loss of function of the encoded protein merlin and activation of mammalian target of rapamycin (mTOR) pathway signaling in *NF2*-deficient cells. Here we describe a gene replacement approach through direct intratumoral injection of an adeno-associated virus vector expressing merlin in a novel human schwannoma model in nude mice. In culture, the introduction of an AAV1 vector encoding merlin into CRISPR-modified human *NF2*-null arachnoidal cells (ACs) or Schwann cells (SCs) was associated with decreased size and mTORC1 pathway activation consistent with restored merlin activity. *In vivo*, a single injection of AAV1-merlin directly into human *NF2*-null SC-derived tumors growing in the sciatic nerve of nude mice led to regression of tumors over a 10-week period, associated with a decrease in dividing cells and an increase in apoptosis, in comparison with vehicle. These studies establish that merlin re-expression via gene replacement in *NF2*-null schwannomas is sufficient to cause tumor regression, thereby potentially providing an effective treatment for NF2.

INTRODUCTION

Loss of function of the *NF2* gene, encoding the tumor suppressor protein merlin, is associated with the development of multiple types of hereditary and sporadic nervous system tumors, including schwannomas, meningiomas, and ependymomas therapy.[1,2] Most of these tumors are benign, but some (in particular meningiomas) may have aggressive biological behavior (atypical, malignant), which may be sporadic or secondary to radiation therapy. Germline loss of one *NF2* allele, followed by somatic mutation of the second *NF2* allele, leads to the neurofibromatosis type 2 (NF2) syndrome, a dominantly inherited disorder the hallmarks of which are bilateral vestibular schwannomas (causing deafness, tinnitus, and disequilibrium) with frequent occurrence of meningiomas, and ependymomas. Vestibular schwannomas, in particular, could potentially be treated by intratumoral injection of a gene replacement vector.

The *NF2*-encoded protein, merlin, links plasma membrane receptors to the actin cytoskeleton and modulates signaling pathways related to cell morphology, proliferation, and survival.[3] Its interactions with different signaling pathways are multiple and complex, involving mTORC1/mTORC2,[4–7] receptor tyrosine kinases,[8] Rac/p21-activated

Received 14 January 2022; accepted 17 June 2022;
https://doi.org/10.1016/j.omtm.2022.06.012.

[15]First co-authors

[16]These authors contributed equally

Correspondence: Xandra O. Breakefield, Molecular Neurogenetics Unit, Massachusetts General Hospital-East, 13th Street, Building 149, Charlestown, MA 02129, USA.
E-mail: breakefield@hms.harvard.edu
Correspondence: Vijaya Ramesh, Center for Genomic Medicine, Massachusetts General Hospital, USA; Department of Neurology, Massachusetts General Hospital, 185 Cambridge Street, Boston, MA 02114, USA.
E-mail: ramesh@helix.mgh.harvard.edu

kinase,[9,10] Hippo signaling,[11,12] and a nuclear function regulating the E3 ubiquitin ligase, $CRL4^{DCAF1}$.[13] Merlin interacts with at least 38 other proteins in different contexts.[14–18] Arachnoidal cell (AC), meningioma, Schwann cell (SC), and schwannoma cells lacking merlin show activated mTORC1 signaling, as well as increased proliferation/migration.[4,6,7,19,20] Merlin overexpression in mouse schwannoma cells leads to increased anchorage-independent growth in culture and reduced growth of subcutaneous schwannomas in mice,[21] as well as growth factor-induced micropinocytosis and receptor recycling in merlin-deficient cells in culture.[22]

Current therapy for NF2 schwannomas involving surgery and radiotherapy can be effective for individual tumors but can also result in serious neurologic complications, including loss of nerve function, e.g., post-surgery deafness or facial paralysis in the case of vestibular schwannomas. In addition, while the anti-vascular endothelial growth factor (VEGF) antibody, bevacizumab, displays efficacy for progressive vestibular schwannomas in improving hearing and reducing tumor volume in about 40% of patients,[23] it has limited long-term effects.[24] Thus, the lack of safe, effective, and lasting treatment for *NF2*-deficient tumors presents an unmet medical need.

Gene replacement therapy for hereditary diseases has shown promise for monogenic immunodeficiency diseases,[25] hemophilia,[26] spinal muscular atrophy,[27] and Leber congenital amaurosis,[28] and is in clinical trials for a number of neurologic disorders (for review see Mendell et al.[29]). Moreover, in the nervous system, adeno-associated virus (AAV) vectors can provide efficient gene delivery *in vivo* and long-term (years) expression in non-dividing cells with a high degree of safety. Previously we reported that AAV-mediated delivery of procaspase-1 under a SC-specific promoter led to schwannoma regression in a mouse model.[30,31] Recent studies also support regression of schwannomas using proteins that induce cell death under a Schwann cell-specific promoter.[32–34] The current study demonstrates that AAV-based delivery of functional merlin produces inhibition of mTORC1 activation in human *NF2*-null ACs and SCs in culture. Further, we describe a new sciatic nerve xenograft model in nude mice for schwannomas using human *NF2*-null immortalized SCs for which a single intratumoral injection of the AAV-merlin vector leads to regression of tumors. These studies serve as proof of principle that restored merlin expression in *NF2*-deficient tumor cells has the potential to provide therapeutic efficacy.

RESULTS

Merlin encoded in AAV1 vectors re-introduced into cultured merlin-negative ACs and SCs demonstrates functional effects

Before testing the effect of AAV-mediated merlin expression in *NF2*-null cells, we tested the transduction efficiency of an AAV1 vector encoding GFP (AAV1-GFP) in human ACs and mouse schwannoma cells in culture (Figure S1). We found human *NF2*-null CRISPR-modified arachnoid cells (AC-CRISPR) and mouse *Nf2*-null SC4 SCs were relatively resistant to AAV1-mediated gene delivery. However, we were able to successfully transduce them with AAV1 packaged in association with extracellular vesicles (EVs): exosome-associated AAV (exo-AAV)-GFP.[35] These data paved the way for us to evaluate gene delivery and the function of merlin delivered by exo-AAV vectors to merlin-negative cells in culture.

The cDNA for human *NF2*-isoform 1 (NCBI: NM_000268) was inserted into an AAV plasmid under the strong constitutive chicken β-actin (CBA) promoter followed by an internal ribosome entry site (IRES) and coding sequences for GFP (Figure S2). This vector, AAV-merlin, was produced as exo-AAV1 and used to transduce human *NF2*-null AC-CRISPR cells with GFP at a dose of 6.0×10^4 genome copies (gc)/cell, or merlin at 3.3×10^5 gc/cell, and expression of merlin and reduction in phosphoS6 (S240/4) (pS6) was confirmed by immunoblotting (Figure 1A). We also confirmed the expression of merlin and downregulation of pS6 in *Nf2*-mutant mouse SC4 SCs transduced with exo-AAV1-merlin (Figures S3A and S3B), with merlin known to inhibit this phosphorylation via blockade of the mTORC1 pathway.[4,5] In addition, a FLAG-tagged version of merlin was generated by cloning human NF2-isoform 1 into AAV-CBA-FLAG-woodchuck hepatitis virus post-transcriptional regulatory element (WPRE). Expression of AAV-FLAG-merlin was confirmed in HEK293T cells by immunoblotting (Figures S4A and S4B). Immortalized human SCs, which had been CRISPR modified to disrupt both *NF2* alleles (SC-null),[20] were transfected with the AAV-CBA-FLAG-merlin plasmid and expression was confirmed by immunoblotting with consequent downregulation of pS6 (Figure 1B). Re-introduction of merlin, either by infection of *NF2*-null AC-*CRISPR* cells or by transfection of SC-null cells, was functionality validated by immunoblotting for downregulation of the mTORC1 signaling pathway readout pS6 relative to the parental cells using ImageJ quantitation (Figures 1C and 1D). We also observed normalization of the enlarged cell size, a hallmark of mTORC1 activation, after merlin re-expression in *NF2*-null AC-CRISPR cells (Figure 2A), consistent with the role of merlin in downregulating TORC1 signaling. When *NF2*-null ACs were transduced with the exo-AAV1-merlin vector, their size was reduced to near normal levels as quantitated by ImageJ using staining for F-actin, a structural component distributed throughout the cells as a correlate for cell area/size (Figure 2B).

Injection of AAV1-CBA-FLAG-merlin into human schwannoma tumors in the sciatic nerve of nude mice inhibits their growth and can lead to regression

Human immortalized SCs, both SC-wild type (WT) and SC-*NF2*-null, were stably transduced with a lentivirus vector encoding firefly luciferase (Fluc) and mCherry,[30] hence termed SC-WT-FC and SC-null-FC. Each cell type was injected into the sciatic nerve of nude (*nu/nu*) mice, as described,[36] with an experimental overview shown in Figure 3A. Tumor growth was monitored by bioluminescence imaging (BLI) over a 14-week period. The SC-WT-FC cells were eliminated by 8 weeks, as shown by loss of BLI over this period (Figure S5). In contrast, the SC-null-FC cells formed BLI-positive tumors by 4 weeks after implantation (Figure 3B, left panels). Neuropathologic analysis of the sciatic nerves at 14 weeks after implantation of SC-null-FC cells revealed the proliferation of cells and formation of

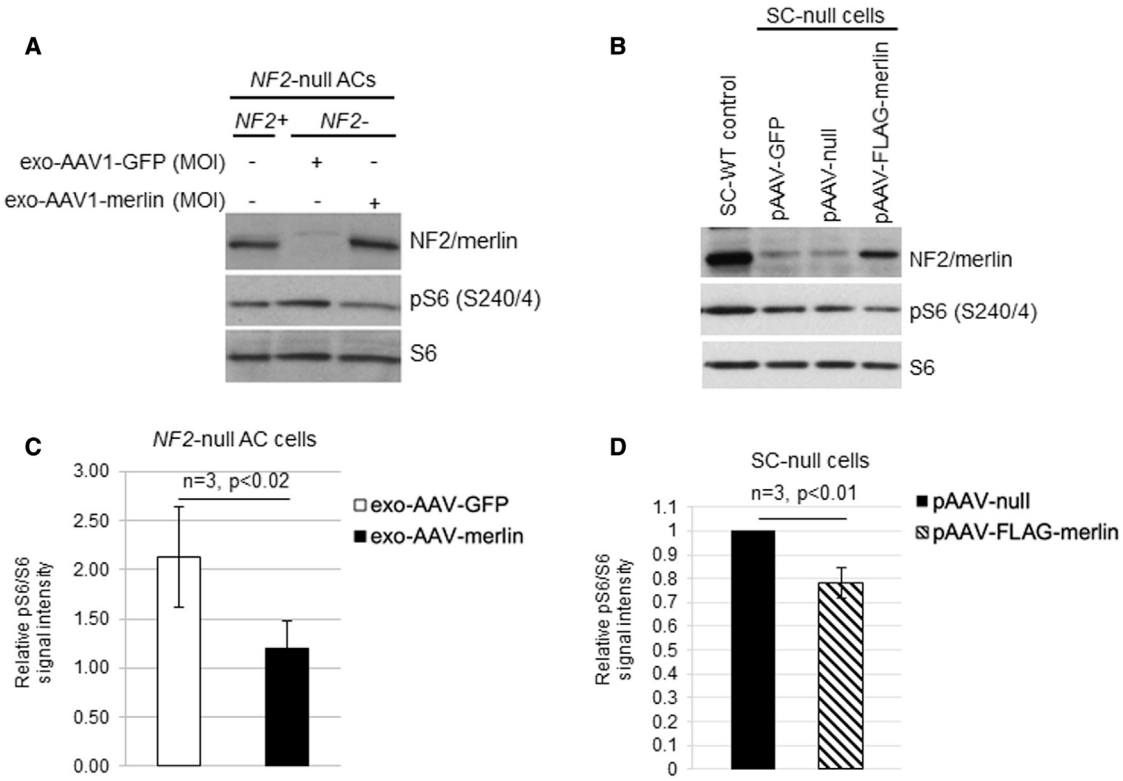

Figure 1. AAV-mediated re-introduction of merlin into *NF2*-null cells leads to downregulation of mTORC1 signaling

(A) Immunoblot shows re-expression of NF2/merlin in human *NF2*-null(–) AC-CRISPR transduced with exo-AAV1-merlin. Re-introduction of merlin led to decreased phosphorylation of ribosomal protein S6 (pS6 S240/4; mTORC1 pathway readout) compared with exo-AAV1-GFP control. Dosing of exo-AAV1-GFP was 5×10^4 gc/cell and exo-AAV1-merlin was 3.3×10^5 gc/cell. (B) Immunoblot of human SC-null cells transiently transfected with pAAV-FLAG-merlin plasmid led to decreased pS6 (S240/4) compared with pAAV-null plasmid. A representative image for transfections using 5 μg of each plasmid is shown. *NF2*-expressing SC-WT control cells and pAAV-GFP-transfected cells are also shown. (C) Quantitation of immunoblotting using Fiji/ImageJ for pS6 (S240/244) relative to total S6 for *NF2*-null ACs transduced with exo-AAV1-merlin is shown normalized to *NF2*+ ACs = 1 (n = 3; error bars, mean ± SD; $p < 0.02$). (D) Quantitation of immunoblotting for SC-null cells transfected with 4–10 μg pAAV-null or pAAV-FLAG-merlin plasmid is shown normalized to pAAV-null empty vector (n = 3; error bar, mean ± SD; $p < 0.01$).

tumors with disruption and expansion of the nerves (in contrast to normal nerve histology in controls) (Figure 4). Tumors showed increased proliferation (highlighted with Ki67 immunohistochemistry) and patchy expression of SC proteins, S100, and SOX10.

Once tumor growth of the SC-null-FC cells was observed (4 weeks after implantation of cells), as assessed by *in vivo* BLI, tumors were injected with AAV1-CBA-FLAG-merlin (see Figure S4A for diagram of vector construct) at a single dose of 4×10^8 gc in 2 μL of phosphate buffered saline (PBS) or with 2 μL of PBS. The growth of tumors was monitored over the following 10 weeks by *in vivo* BLI and the results were averaged (Figure 3C). Out of nine tumors treated with AAV1-FLAG-merlin, seven tumors totally regressed, one stayed the same size as prior to vector injection, and one grew, while all grew in the PBS-treated mice (Table 1 and 2). The overall health of all the animals was good, with normal weight and motility.

At the end of the experiment (week 14) tumors were harvested and analyzed by neuropathology using hematoxylin and eosin (H&E) staining, and immunohistochemistry for Ki67, SOX10, and S100. The schwannomas injected with PBS and stained for H&E (Figure 5A) showed an expansion of the sciatic nerve as the tumor infiltrated and diffused into the nerve bundles, forming clusters. Intraneural inflammation and hypercellularity were also noticeable with an atypical mixture of cells present throughout the nerve. Ki67 immunostaining of the PBS-treated tumor similarly showed proliferation of cells intraneurally as well as perineurally (Figure 5C), with rate-positive SOX10 and S100 cells scattered throughout (Figures 5E and 5G) the massively expanding nerve with the infiltrating tumor cells displacing axons peripherally.

Following the treatment of the schwannoma tumor with AAV1-FLAG-merlin vector, H&E staining shown that the tumor was regressed, with some atypical cells and some mild hypercellularity still present (Figure 5B). Ki67 immunostaining confirmed the resolution of cell proliferation with some lymphocytes seen (Figure 5D). This was validated by the significant decrease in the percentage of Ki67-positive cells in merlin vector-treated tumors,

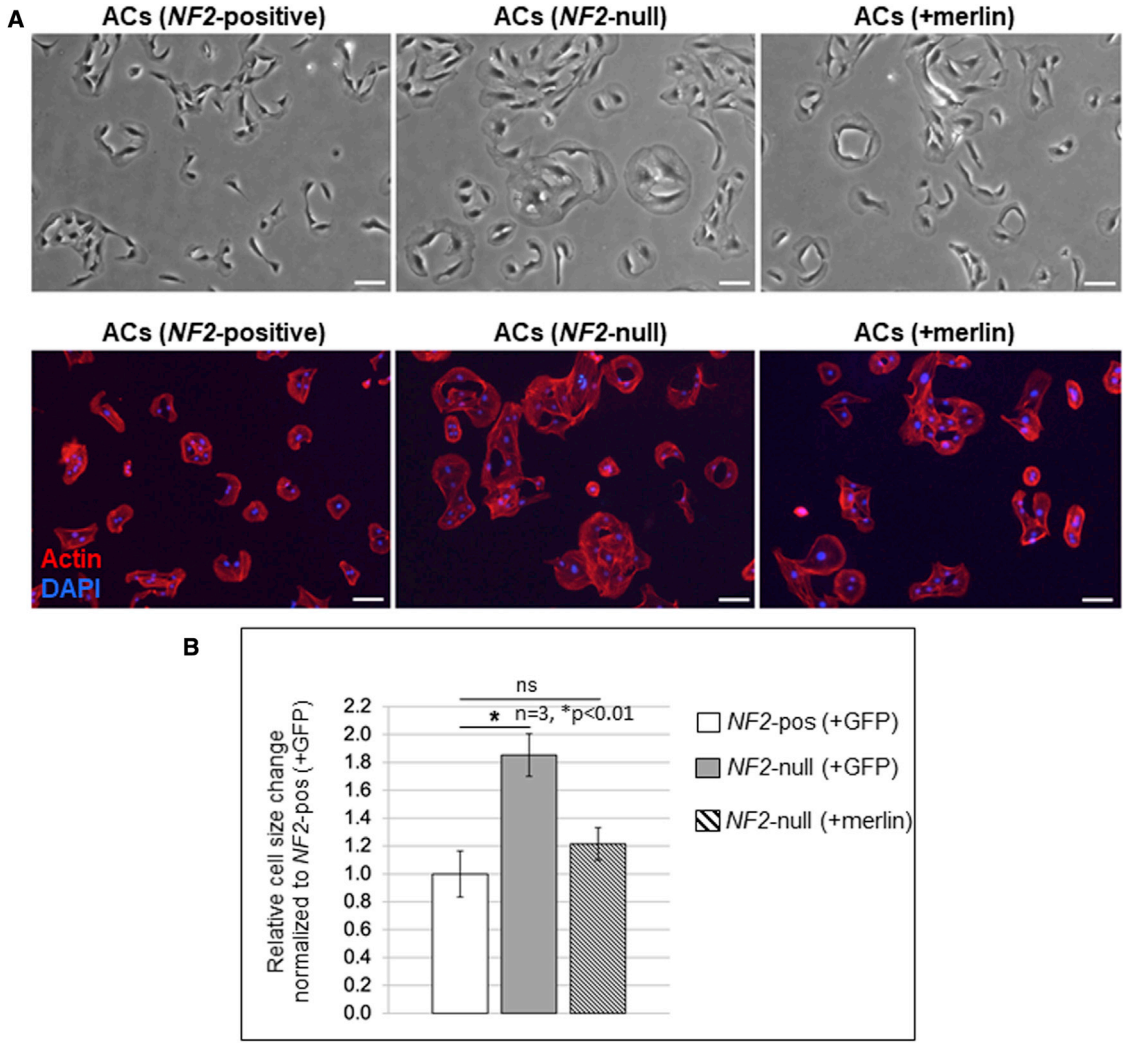

Figure 2. Reintroducing merlin into NF2-null human ACs decreases enlarged cell size

(A) Representative bright field images (top) and fluorescent staining images (bottom) for total actin (red) and nuclear DAPI (blue) to mark each cell show *NF2* positive ACs transduced with exo-AAV1-GFP (+GFP) (left) along with enlarged *NF2*-null ACs (+GFP) (center). Re-introduction of merlin into the *NF2*-null ACs with exo-AAV1-merlin revealed a decrease in cell size (right). (B) Quantitation using Fiji/ImageJ of relative change in cell size was determined by actin staining/cell. Data are plotted as average of total actin-positive staining/cell in three fields (median of ~100–150 cells/field) for each condition, normalized to *NF2*-positive ACs (+GFP). Error bars, mean ± SD; *p < 0.01; ns, not significant.

compared with PBS-treated tumor (Figure S6). With SOX10 and S100 staining, the merlin vector-treated nerve appeared nearly normal with intact architecture and tightly packed myelinated axons running longitudinally (Figure 5F and 5H). A small perineural area of hypercellularity and some intraneural nodules displacing axons (the latter only seen with S100 staining) might potentially constitute some remnants of the tumor. Tumors regressed at least in part through apoptosis with an average of about 18% of the cells TUNEL positive in AAV-merlin-injected tumors and less than 5% in AAV-null-injected tumors after 8 days, which was a significant difference, with essentially no TUNEL-positive cells in naive nerve (Figure S7).

Following injection of AAV1-FLAG-merlin vector into a schwannoma in the sciatic nerve, the presence of vector DNA in genomic DNA was confirmed (Figure S8) and the expression of RNA encoded in the vector was detected 8 days following injection into the sciatic nerve (Figure S9) and into tumor in sciatic nerve (Figure S10). In a small sample size, tumors in the sciatic nerve injected with AAV1-null vector did not regress (Figure S11).

DISCUSSION

Our studies support suppression, and even regression, of human schwannoma growth *in vivo* by *NF2* gene replacement in a preclinical xenograft mouse model. Promising aspects of this approach are that it

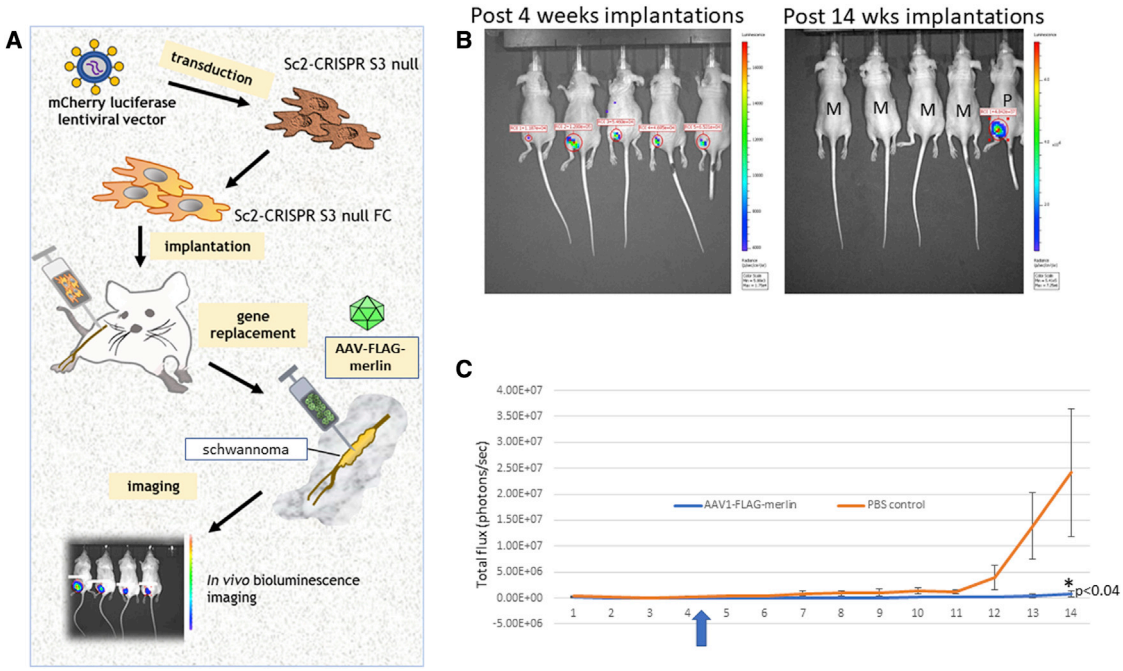

Figure 3. Growth of human NF2-null schwannoma tumors with and without vector injection

(A) Schematic representation of the generation of the mouse model bearing human NF2-null schwannomas. (B) Bioluminescence imaging (BLI) of the mice with tumor signals. Four weeks after implantation of SC-null-FC cells (30,000) in the sciatic nerve (left, before vector injection) and 14 weeks after implantation (right, after vector injection at week 4–5); M, AAV-merlin injected; P, PBS injected. (C) Human schwannoma cells (SC-null-FC; 30,000) were implanted into the sciatic nerves of nude mice (n = 18) and the growth of tumors was measured by BLI. At 4–5 weeks post implantation, mice were either injected intratumorally with 4×10^8 gc AAV1-FLAG-merlin vector (n = 9; blue line) or PBS as control (n = 9; orange line). See Tables 1 and 2 for BLI values.

is effective over an extended period of at least months after a single intratumoral injection, and that AAV vectors are proving beneficial without adverse effects in clinical trials for a number of other human diseases. The cessation of tumor growth appears to occur by merlin-dependent inhibition of proliferation and apoptosis of schwannoma cells. Studies by Ahmad et al.[37] have shown that merlin expression facilitates apoptosis mediated by the low-affinity neurotrophin receptor, p75-NTR in SCs as a result of nerve damage. Neuropathologic and health evaluation indicated no toxic effects to the animals by intratumoral merlin vector treatment. Given the limitations of surgery and radiotherapy to control these tumors in patients, the need for continuous treatment, and the side effects of drugs used to control schwannoma growth, gene therapy is a promising new therapeutic avenue.

The effectiveness of a single intratumoral injection of AAV1-merlin into this human schwannoma model in inhibiting the overall growth of the tumors in immunocompromised mice seems unexpected given that typically AAV vectors only transduce a subset of cells at the injection site. We hypothesized that overexpression of merlin in these null cells would lead to cell shrinkage, apoptosis, and/or inhibition of proliferation, but still many tumor cells would not receive the transgene and should continue to divide. If, however, merlin expression in *NF2*-deficient cells inhibits their proliferation shortly after transduction, they should continue to express merlin for a prolonged period of time, possibly at abnormally high levels under the CBA promoter. The overall apparent cessation of growth of tumors after merlin transduction of a subset of cells suggests that this merlin-dependent inhibition of cell proliferation may have a "bystander effect," with transduced schwannoma cells able to suppress the growth of non-transduced cells within the tumor. This could happen if merlin was incorporated into the EVs secreted by transduced cells overexpressing merlin, with these EVs being taken up by surrounding cells. Previous studies have shown that overexpressed proteins are typically released from cells within EVs and are taken up and can be functionally active in recipient cells (e.g., Hall et al.[31] and Mizrak et al.[38]).

Given the broad activity of merlin in various cell signaling pathways, the many proteins with which it interacts, and its expression in many cell types, it is difficult to predict what effects elevated expression of merlin would have on normal cell types. Although direct injection of a vector into the tumor in the sciatic nerve would restrict infection primarily to the schwannoma cells, a small fraction of vector will undoubtedly infect surrounding SCs, and endothelial cells, as well as neurons in the dorsal root ganglia by retrograde transport. An even smaller portion of the vector would enter the vasculature and could infect other cell types throughout the body. Uptake into cells that are susceptible to tumor formation in NF2

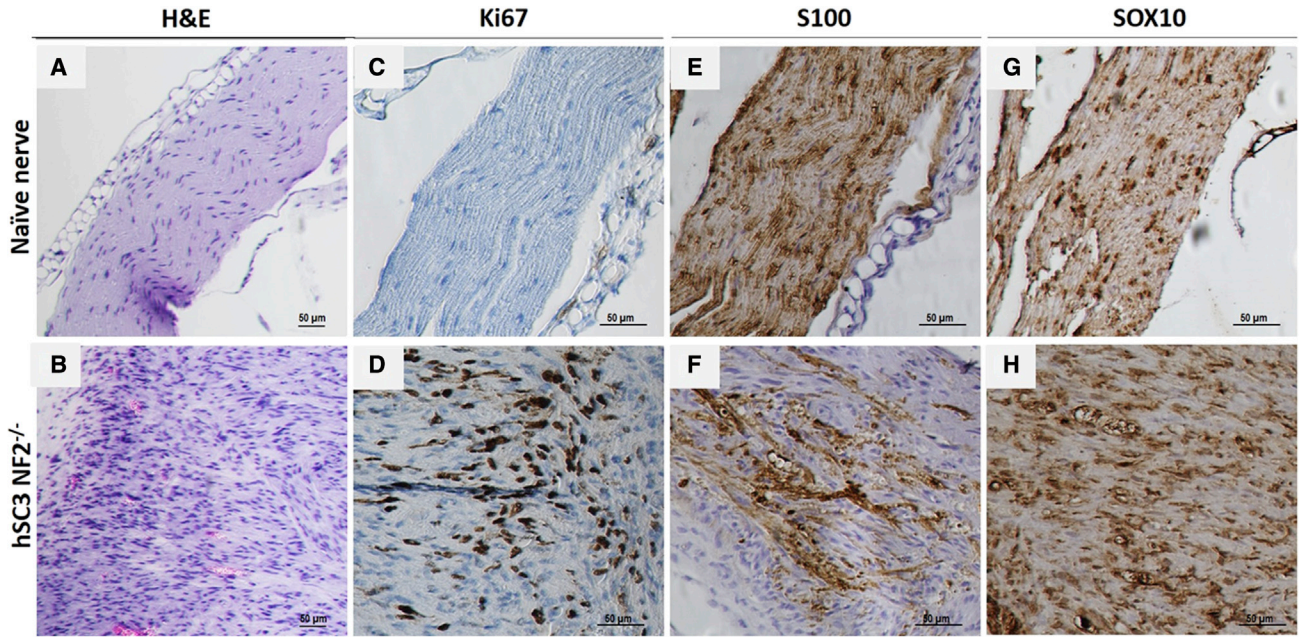

Figure 4. Neuropathology of normal nerve and SC-null-FC schwannoma

Establishment of schwannoma tumor model via implantation of immortalized SC-null-FC cells directly into the sciatic nerve of immunodeficient mice with neuropathologic evaluation. (A) H&E staining of longitudinal sections of naive nerve, and (B) nerve post implantation (14 weeks) of SC-null-FC schwannoma cells. (C) In naive nerve, we detected no KI67-positive cells, (D) while many Ki67-positive SC-null-FC cells were detected in the schwannoma. (B and F) As compared with the naive nerve, the tumor-bearing nerve also exhibited disrupted architecture caused by proliferating tumor cells growing and displacing the few remaining myelinated axons (S100 positive). (E) Expression of Schwann cell marker SOX10 was detected in the normal nerve and (H) in the implanted SC-null-FC schwannoma cells.

patients, such as SCs (forming schwannomas), ACs (meningiomas), and ependymal cells (ependymomas) might actually prevent future instigation of tumor formation in the event they underwent a subsequent somatic mutation in the normal *NF2* allele of *NF2* mutant gene carriers. It is currently not possible to titrate the level of expression of the transgene and we have selected high level expression to inhibit tumor growth, thus it remains an issue as to whether the vector could have toxic effects on some normal cells. In these studies, we observed no detrimental effects on the health of mice injected intratumorally with the AAV1-merlin vector. Still, more detailed biodistribution and toxicity studies would be required in follow-up preclinical toxicology studies before consideration of clinical trials. If toxicity to other cell types is found, merlin could be expressed under a SC-specific promoter, such as for P0[30,34] or periostin.[39]

NF2 is a single-gene disorder and gene replacement has the potential to treat the "driver" mutation, which cannot be targeted in any other way (e.g., current pharmacology is good at inhibiting overactive pathways, but not replacing tumor suppressor genes). This approach can treat the tumors (as shown in our data), but may also be able to inhibit future tumor formation by transducing $NF2^{+/-}$ heterozygous cells (i.e., be used as a preventative prophylactic gene therapy). This approach represents a fundamentally new treatment for NF2, not just trying to treat aspects of tumor biology, such as treatment with bevacizumab, everolimus, and so forth do.

In addition, this AAV-merlin strategy can be tested in other benign schwannoma models, such as the *Nf2*-floxed mouse crossed to transgenic mice expressing Cre under control of the periostin promoter active in SC progenitors, which forms vestibular schwannomas.[39] Other mouse orthotopic allograft schwannoma models are also available.[40,41] It will be important to evaluate whether overexpression of merlin using an AAV vector can inhibit growth of schwannomas without mutations in *NF2*, and other types of meningiomas[42] and ependymomas[43] in mouse models. There may also be ways to expand the effectiveness of this therapeutic paradigm by promoting the transfer of merlin via EVs or by injecting the vector into biofluids with broader access to tumors throughout the body, including intravenous and intrathecal injections. Even in cases where surgical removal of a tumor is needed, e.g., a vestibular schwannoma causing hearing loss, carrying this out in combination with injection of AAV-merlin could limit the extent, time, and risks of surgery, which include deafness and facial paralysis associated with resection of vestibular schwannomas and the subsequent regrowth of the tumor, thus providing benefit to patients. This study provides a new modality in the therapeutic armamentarium to reduce size of NF2-related tumors in the nervous system, an approach that can be combined with other current treatments.

MATERIALS AND METHODS

Cell lines

Human *NF2*-WT and *NF2*-null ACs, isogenic clones from an immortalized human AC line modified by CRISPR-Cas9 genome editing

Table 1. BLI values for individual mice bearing human schwannoma injected with AAV1-FLAG-merlin

Post injected	1	2	3	4	5	6	7	8	9
1 week	1.14E+04	7.71E+04	1.42E+04	1.40E+05	2.06E+05	9.56E+04	4.26E+05	1.74E+05	2.11E+04
2 weeks	1.19E+04	5.46E+04	2.43E+04	1.64E+05	4.91E+04	1.87E+04	6.37E+04	8.65E+04	1.11E+04
3 weeks	0.00E+00	0.00E+00	6.22E+04	2.76E+05	4.25E+04	4.22E+04	1.39E+04	2.39E+04	1.65E+04
4 weeks	3.81E+04	4.48E+04	6.85E+04	2.50E+05	1.72E+05	5.93E+04	1.04E+05	4.04E+04	1.97E+04
5 weeks	7.71E+04	8.76E+04	6.80E+04	2.46E+05	1.19E+04	5.64E+04	1.03E+05	3.90E+04	1.50E+04
6 weeks	8.63E+04	0.00E+00	5.64E+04	2.28E+05	0.00E+00	5.50E+04	1.03E+05	2.89E+04	0.00E+00
7 weeks	5.59E+04	0.00E+00	4.04E+04	2.28E+05	0.00E+00	5.03E+04	1.02E+05	2.34E+04	0.00E+00
8 weeks	0.00E+00	0.00E+00	0.00E+00	0.00E+00	0.00E+00	4.81E+04	1.02E+05	2.21E+04	0.00E+00
9 weeks	0.00E+00	0.00E+00	0.00E+00	0.00E+00	0.00E+00	4.75E+04	1.01E+05	2.19E+04	0.00E+00
10 weeks	0.00E+00	0.00E+00	0.00E+00	0.00E+00	0.00E+00	4.54E+04	4.03E+04	8.55E+05	0.00E+00
11 weeks	0.00E+00	0.00E+00	0.00E+00	0.00E+00	0.00E+00	4.48E+04	3.50E+04	1.16E+06	0.00E+00
12 weeks	0.00E+00	0.00E+00	0.00E+00	0.00E+00	0.00E+00	4.37E+04	0.00E+00	1.20E+06	0.00E+00
13 weeks	0.00E+00	0.00E+00	0.00E+00	0.00E+00	0.00E+00	2.88E+04	0.00E+00	2.98E+06	0.00E+00
14 weeks	0.00E+00	0.00E+00	0.00E+00	0.00E+00	0.00E+00	2.34E+04	0.00E+00	5.28E+06	0.00E+00

Vector was injected at post 4 weeks.

(AC-CRISPR lines), and *NF2* expressing or *NF2* null have been previously described.[7] The immortalized human SC line (pn02.3)[44] (hereafter referred to as SC-WT) underwent CRISPR-mediated genome editing to disrupt both *NF2* alleles creating the knockout S3-null line (referred to here as SC-null).[20] The parental SC-WT and SC-null lines were stably transduced with a lentivirus encoding Fluc and mCherry.[45] The *Nf2*-mutant mouse SC line SC4 has been previously described.[46] HEK-293T human embryonic kidney cells (from M. Calos, Stanford University, Stanford, CA), SC-WT, SC-null, SC4, and AC-CRISPR lines were grown in Dulbecco's modified Eagle's medium (DMEM). Growth media were supplemented with either 10% fetal bovine serum (FBS; Sigma-Aldrich, St. Louis, MO) for HEK-293T, SC-WT, SC-null, and mouse SC4 cells, or 15% FBS for AC-CRISPR lines, and 1% penicillin-streptomycin (Cellgro, Herndon, VA). Cells were maintained at 37°C in a controlled atmosphere of 5% CO_2 and 95% relative humidity.

Conventional AAV and exo-AAV production

For transgene expression studies with AAV vectors, the following constructs were employed: (1) AAV expression plasmid, pAAV-CBA-GFP (a gift from Miguel Sena-Esteves, UMass Medical Center) containing AAV inverted terminal repeats (ITRs) flanking the CBA expression cassette which consists of a hybrid CMV-IE enhancer/CBA promoter, GFP cDNA, WPRE, and bovine growth hormone and SV40 poly(A) signal sequences (bGH poly(A)); (2) pAAV-CBA-merlin containing the CBA promoter, *NF2* cDNA, an IRES, upstream of GFP cDNA, followed by bGH poly(A) signal sequence; and (3) AAV-CBA-FLAG-merlin containing a FLAG epitope tag fused to the N terminus of merlin followed by a WPRE and bGH poly(A) signal sequence.

AAV vectors and exo-AAV were produced in 293T cells, as previously described.[47,48] Briefly, 293T cells were triple transfected (calcium phosphate method[49]) with (1) AAV rep/cap plasmid (pXR1) encoding AAV2 rep proteins and AAV1 capsid proteins; (2) an adenovirus helper plasmid, pAdΔF6; and (3) the ITR flanked transgene expression cassette in 15-cm dishes. Conventional AAV vectors were isolated from cell lysates and purified by iodixanol density gradient ultracentrifugation. Next, iodixanol was removed and vector concentrated using Amicon Ultra 100 kDa molecular weight cutoff (MWCO) centrifugal devices (Millipore, Billerica, MA) in PBS and finally filtered through a 0.22-μm Millex-GV Filter Unit (Millipore).

For exo-AAV, medium was changed to DMEM with 2% EV-free FBS (made by overnight 100,000 × *g* centrifugation of serum to deplete bovine EVs). At 72 h post transfection, medium was harvested. Cell debris and apoptotic bodies were removed by sequential 10 min 300 × *g* and 2,000 × *g* centrifugations. The supernatant containing exo-AAV was then centrifuged at 20,000 × *g* for 1 h to deplete larger microvesicles. Next, the remaining medium was centrifuged at 100,000 × *g* for 1 h using a Type 70 Ti rotor in an Optima L-90K ultracentrifuge (both Beckman Coulter, Indianapolis, IN). The resulting pelleted material was resuspended in serum-free DMEM. Both exo-AAV and conventional AAV preparations were stored at −80°C.

To ensure accurate titration of exo-AAV, which contains protein and lipids, we purified AAV genomes using High Pure Viral Nucleic Acid Kit (Roche, Indianapolis, IN). This kit contains detergents and proteinase K to degrade and lyse membrane viruses and is also certified to remove PCR inhibitors. Before kit purification, plasmid DNA from the transfection was removed by mixing 5 μL of the exo-AAV samples with 1 μL of DNase I, 5 μL of 10× buffer, and 39 μL of water. Samples were incubated for 1 h at 37°C and then DNase I was inactivated at 75°C for 15 min. Next, AAV and exo-AAV preparations were titered

Table 2. BLI values for individual mice bearing human schwannoma injected with PBS

Post injected	1	2	3	4	5	6	7	8	9
1 week	1.08E+04	1.43E+04	3.37E+05	1.02E+05	0.00E+00	7.10E+05	7.70E+04	1.55E+05	3.16E+05
2 weeks	6.55E+04	2.44E+04	4.70E+04	6.90E+04	7.53E+04	1.79E+04	4.02E+04	1.43E+05	2.83E+04
3 weeks	7.24E+04	6.24E+04	4.05E+04	0.00E+00	6.15E+04	3.83E+04	2.70E+04	1.46E+05	5.19E+04
4 weeks	8.02E+04	6.86E+04	2.41E+04	0.00E+00	0.00E+00	6.08E+04	1.71E+05	8.04E+05	9.87E+04
5 weeks	8.32E+04	6.92E+04	2.18E+05	1.32E+05	4.42E+05	6.22E+04	1.08E+05	8.18E+05	3.27E+05
6 weeks	9.91E+04	5.64E+05	1.51E+05	1.30E+05	9.35E+04	2.65E+05	2.01E+05	8.42E+05	4.28E+05
7 weeks	1.66E+05	1.04E+06	1.07E+05	1.87E+05	3.56E+05	3.47E+05	2.64E+05	4.04E+06	4.75E+05
8 weeks	1.79E+05	1.87E+05	1.09E+05	3.48E+05	4.32E+05	4.56E+05	3.20E+05	4.10E+06	5.27E+05
9 weeks	1.81E+05	3.48E+05	1.81E+05	3.98E+05	4.64E+05	4.74E+05	3.86E+05	4.87E+06	5.37E+05
10 weeks	1.98E+05	4.99E+05	1.98E+05	4.99E+05	7.69E+05	5.31E+05	3.90E+05	4.96E+06	1.23E+06
11 weeks	2.70E+05	5.19E+05	2.70E+05	5.19E+05	7.72E+05	6.81E+05	2.55E+06	dead	2.25E+06
12 weeks	4.70E+05	6.55E+05	4.70E+05	6.55E+05	3.47E+06	7.70E+05	3.87E+06		1.66E+07
13 weeks	5.72E+05	7.62E+05	5.72E+05	7.62E+05	8.33E+06	8.46E+05	3.24E+07		3.79E+07
14 weeks	6.62E+05	1.84E+06	6.62E+05	1.84E+06	1.54E+07	1.80E+06	3.77E+07		8.33

Vector was injected at post 4 weeks.

using a quantitative TaqMan PCR that detects AAV genomes (bGH poly(A) region of the transgene cassette).[47]

Transduction of cells in culture and evaluation of GFP and merlin expression

Human *NF2*-null AC-CRISPR and mouse SC4 cells were transduced with exo-AAV1-GFP at a dose of 5.0–6.0 $\times$ 10^4 gc/cell or exo-AAV1-merlin at 3.3–5.0 $\times$ 10^5 gc/cell. Spin-infection was carried out using 1 $\times$ 10^5 cells/well in 12-well plates at 820 $\times$ *g* for 20 min at room temperature, followed by incubation at 37°C overnight. The following day, cells were seeded into six-well plates (for immunoblotting) or into 12-well plates containing coverslips (for immunofluorescence [IF] staining of AC-CRISPR cells). At 72 h post transduction, cells were visualized microscopically for GFP fluorescence and lysed for immunoblotting, or coverslips were fixed in 4% paraformaldehyde (Electron Microscopy Sciences, Hatfield, PA) at room temperature for 20 min.

Transfection AAV-FLAG-merlin in HEK-293T and SC-null cells in culture

Transfection of HEK-293T cells was performed to test/optimize expression of AAV-CBA-FLAG-merlin, compared with *NF2/merlin* (isoform 1) cloned into the mammalian expression vector pcDNA3, expressing a 5′-FLAG tag, which we have previously reported.[50] Transfection was carried out using Lipofectamine 2000 reagent (Invitrogen), according to manufacturer's instructions. Briefly, 1 $\times$ 10^6 cells were seeded onto 6-cm culture dishes followed by transfection with empty pcDNA3-5′FLAG, merlin-pcDNA3-5′FLAG, or AAV-FLAG-merlin. At 48 h post transfection, cells were harvested for immunoblotting. *NF2*-null CRISPR-modified SC (SC-null) cells were transiently transfected with AAV-GFP, empty AAV (AAV-null), or AAV-FLAG-merlin plasmid. Transfection was carried out using Lipofectamine Stem reagent (STEM00003, Invitrogen) according to manufacturer's instructions. Briefly, 2.5 $\times$ 10^5 cells were seeded in each well of a six-well plate. The day after seeding, 4 μg, 5 μg, or 10 μg of plasmid was used for transfection. At 24 h post transfection, medium was changed for fresh growth medium to remove complexes, and, at 48 h post transfection, cells were harvested for immunoblotting.

Morphological analysis

For evaluation of cell size by IF staining, cells were permeabilized with 0.2% Triton X-100/2%BSA/PBS for 20 min at room temperature followed by actin staining with AlexaFluor594-conjugated phalloidin (Life Technologies, Grand Island, NY), then mounted on coverslips using Prolong Gold antifade reagent with DAPI (Invitrogen). Visualization and imaging of actin staining as well as AAV1-GFP expression in live cells was carried out on a Nikon (Tokyo, Japan) Eclipse TE2000-U inverted microscope using the EXFO X-Cite 120 fluorescent illumination system. Images were acquired with a Nikon DS-QiMc camera and NIS-Elements BR imaging software. Cell size analysis of actin staining was carried out using ImageJ/Fiji open source image processing and analysis software.[51]

Immunoblotting

For immunoblotting, cells were lysed in RIPA lysis buffer (50 mM Tris, pH 8.0, 150 mM NaCl, 1% Igepal, 0.5% deoxycholate, 0.1% SDS) containing 1× HALT phosphatase inhibitor cocktail (Thermo Scientific, Waltham, MA) and a 1× complete protease inhibitor cocktail (Roche). Cell lysis, SDS-PAGE, and immunoblotting were carried out as described.[4] NF2/merlin polyclonal C26 antibody was diluted at 1:200 in 1% milk/TBS-T (TRIS-buffered saline with 2% Tween 20), as described.[18] Antibodies for phospho-S6 (S240/244) and S6 (Cell Signaling Technology, Danvers, MA) were diluted at 1:1,000 in 5%

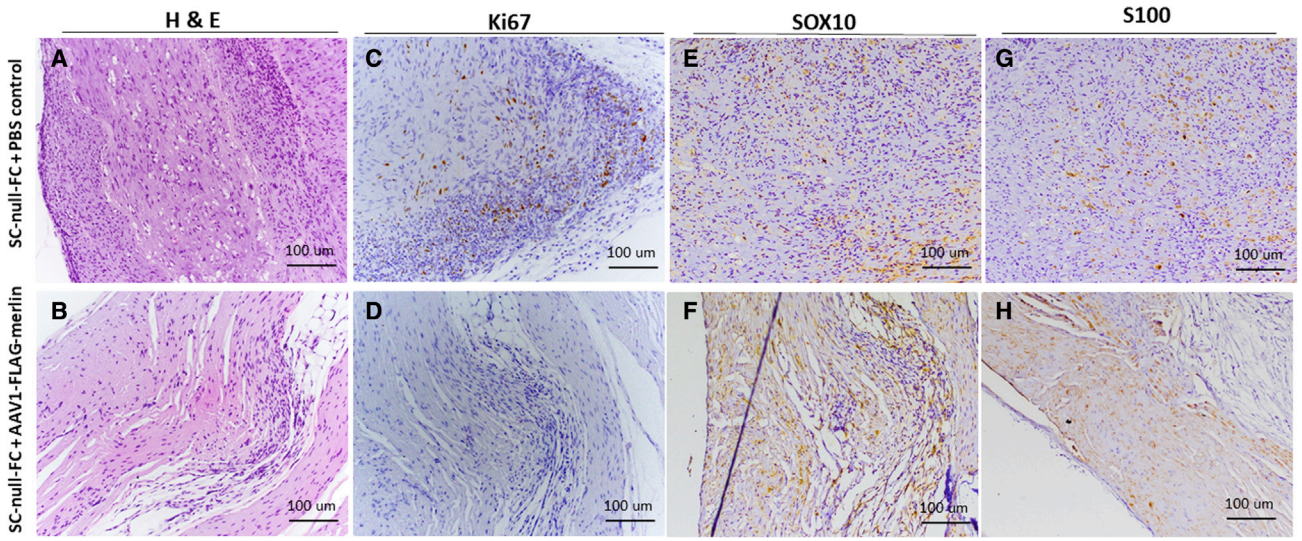

Figure 5. Neuropathology in treated and untreated tumors at 14 weeks

Pathologic analysis of schwannomas for H&E, Ki67, S100, and SOX10 in the sciatic nerve of immunodeficient mice after 10 weeks of treatment with AAV1-FLAG-merlin vector and or PBS. (A) H&E staining of longitudinal sections of the PBS-treated tumors shows nerve expansion, intraneural inflammation, and hypercellularity, with tumor infiltrating and diffusing into the nerve bundles and forming clusters. (B) H&E staining of longitudinal sections of the AAV-merlin-treated tumors shows resolution of the tumor with some atypical cells remaining and a very mild hypercellularity still present. (C) Ki67 staining of longitudinal sections of PBS-treated tumors shows excessive proliferation of cells intraneurally, as well as perineurally. (D) Ki67 staining of longitudinal sections of the AAV-merlin-treated tumors shows resolution of cell proliferation with some lymphocytes present. SOX10 and S100 staining of longitudinal sections of (E and G) the untreated tumors shows a massively expanding nerve and an intraneural tumor that is displacing axons peripherally; rare scattered positive SOX10- and S100-stained cells are visible, but much of the tumor is dedifferentiated (negative staining). (F and H) SOX10 and S100 staining of longitudinal sections of the PBS-treated tumors shows extensive disruption of nerve fibers, while AAV-merlin-treated tumors show a normal-appearing nerve with intact architecture and tightly packed myelinated axons running longitudinally in most parts of the nerve; a small perineural area of hypercellularity might potentially constitute some remnants of the tumor; microscopic intraneural nodules of remnant tumor displacing axons are seen with S100, but not SOX10 staining.

BSA/TBS-T. Anti-FLAG M2 antibody (Sigma) was diluted at 1:2,000 in 2% milk/TBS-T. Secondary antibodies included HRP-conjugated anti-rabbit IgG (Cell Signaling Technology) and HRP-conjugated anti-mouse IgG (VWR International, Radnor, PA). The quantitation of immunoblotting was carried out using ImageJ/Fiji open source image processing and analysis software.[51]

Animals

Experimental research protocols were approved by the Institutional Animal Care and Use Committee (IACUC) for the Massachusetts General Hospital (MGH) following the guidelines of the NIH's Guide for the Care and Use of Laboratory Animals. Experiments were performed on *nu/nu* mice (Charles River Laboratories, Wilmington, MA) kept on a 12:12 light-to-dark cycle with *ad libitum* access to food and water. Male and female nude mice (*nu/nu*) 4–6 weeks old (n = 18) were used for SC cells or vehicle injections into the sciatic nerve unilaterally. Animals were checked daily to evaluate health and sacrificed according to approved protocols if in distress.

Generation of vector injections, bioluminescence monitoring of tumor size, and statistical analysis

Human SC-WT or SC-NF2-null cells were injected directly into the sciatic nerve of isoflurane-anesthetized mice, as described.[36] Specifically, cells were implanted approximately 4 mm distal to the sciatic notch at a point midway between the sciatic notch and the trifurcation of the sciatic nerve into the common peroneal, tibial, and sural branches. Cells were first trypsinized and rinsed, and 30,000 cells in 2 μL of culture medium were injected into the distal sciatic nerve of athymic nude mice (*nu/nu*, 4–6 weeks old males and females; National Cancer Institute [NCI]) using a glass micropipette and a gas-powered microinjector (IM-300; Narishige, Tokyo, Japan). Tumor growth was monitored by *in vivo* BLI at weekly intervals, as described.[45] Briefly, mice were injected intraperitoneally with the Fluc substrate D-luciferin and, 5 min later, signal was acquired with a high-efficiency IVIS Spectrum (Caliper Life Sciences, Hopkinton, MA) under an XGI-8 gas anesthesia system (Caliper Life Sciences). After 4 weeks, tumors that grew progressively were injected with AAV1-CBA-FLAG-merlin (4×10^8 gc) in 2 μL of PBS. Volumetric changes in tumors were tracked by *in vivo* BLI out to 10 weeks post vector injection.

Neuropathology of tumors and surrounding nerve fiber

Mice were perfused with 1× PBS, and sciatic nerves were harvested and subjected to standard histological processing. Nerves were placed in 10% formalin in PBS for 24 h before being dehydrated in graded solutions of alcohol and xylene and embedded in paraffin. After embedding, 6-μm sections were cut with a microtome (Leica RM2155, Nussloch, Germany) and mounted on charged and precleaned Probe-On Plus microscope slides (Fisher Scientific,

Pittsburgh, PA). H&E staining was performed on tissue sections by standard protocol by the MGH Pathology Core. For immunostaining of tissue sections, tissue was deparaffinized, hydrated, and stained. Tissue sections (6 μm) were then permeabilized in sodium citrate, pH 8.0 water bath at 35.0°C–36.1°C (95–97°F) for 30 min for antigen retrieval, washed three times with PBS, and treated with blocking buffer (3% BSA/PBS or 5% milk in 3% BSA/PBS) at room temperature) for 1 h. Staining for S100, Ki67, and SOX10 was performed with a mouse monoclonal S100 antibody (Life Technologies, CA MA1-26621), rabbit monoclonal Ki67 antibody (Ventana #790–4286), or mouse monoclonal SOX10 antibody (Abcam, #ab216020). Sections were stained with the primary antibody (diluted in 1% BSA/PBS 1:10 for S100; 1:50 for Ki67, 1:25 for SOX10) and then applied to tissue sections overnight at 4°C. After the primary antibody incubation, tissue was washed three times with PBS. The secondary antibody DAKO Mouse/Rabbit HRP Kit with horseradish peroxidase (HRP) was applied to the tissue for 30 min at room temperature. After incubation with secondary antibody, the tissue was rinsed three times in PBS and developed in DAKO Rabbit/Mouse Kit with DAB (1 mL of buffer plus one drop of chromagen) for 2 min at room temperature, terminated with water, counterstained with hematoxylin, and dehydrated through grades of alcohol and xylene before being mounted with glass coverslips.

TUNEL staining was performed on tissue sections with the ApopTag Peroxidase *In Situ* Apoptosis Detection Kit (S7100; Millipore) by the MGH Pathology Core. Briefly, sections (6 μm) were baked overnight and deparaffinized in xylene. Then the samples were sequentially rehydrated in 100%, 90%, and 70% ethanol. Permeabilization was performed with proteinase K (S3020; DAKO, Carpinteria, CA, USA) at a dilution of 1:10. After permeabilization, terminal deoxynucleotidyl transferase (TdT), diluted 1:16 in reaction buffer, was applied to each slide and incubated for 1 h at 37°C. Thereafter, the slides were submerged in stop/wash buffer for 10 min. Following washes, digoxigenin HRP-conjugated antibody was applied for 30 min. Apoptotic cells were detected after incubation in the 3,3′-diaminobenzidine chromogen (DAKO) for 3 min and slides were counterstained with hematoxylin. The data were collected from images scanned at ×40 resolution. TUNEL-positive cells were counted manually by using ImageJ plugins (cell counter notice) for AAV1-merlin-injected sciatic nerves (n = 3), AAV1-null-injected sciatic nerves (n = 3), and naive nerves (n = 3) with five randomly selected fields per mouse. Data are represented as the mean ± SEM. For more than two-group comparison, Kruskal-Wallis test was used, followed by Dunn's multiple comparison test.

Ki67 staining quantification

Quantification of tumor cell proliferation following Ki67 staining (brown) was performed using ImageJ. The percentage of positive cells was calculated as brown divided by the sum of brown and blue (DAPI) cells. Data were plotted as the percentage of Ki67-positive nuclei in five randomly selected fields in the tumor area of the sciatic nerve from three different mice per group, scanned at ×20 resolution. The total number of cells counted per group was 568 for merlin vector-injected tumor, 1,560 for merlin vector-injected naive nerve, 4,126 for PBS-injected tumor, and 1,546 for PBS-injected naive nerve. Statistical analysis was performed using one-way ANOVA. Error bars, mean ± SD; ****$p < 0.0001$.

DNA and RNA extraction, cDNA synthesis, qPCR

The sciatic nerves were flash frozen to determine AAV genome biodistribution and expression of transgene mRNA. Qiagen DNeasy Blood and Tissue Kit (catalog no. 69504) was used to isolate genomic and AAV vector DNA according to the manufacturer's instructions. Total RNA was extracted using the Qiagen miRNeasy Micro Kit (catalog no. 217084), and an additional on-column deoxyribonuclease (DNase) digestion using the Qiagen RNase-free DNase set (catalog no. 79254) was performed to ensure digestion of AAV-merlin genomes. Then, according to the manufacturer's protocol, cDNA was generated consistently with an initial RNA input of 400 ng for all samples, using the SuperScript VILO cDNA Synthesis Master Mix (Thermo Fisher Scientific, catalog no. 11754-050). A cDNA clean-up step was then performed using QIAquick PCR purification kit (catalog no. 5720462). Using 50-ng genomic DNA as template, TaqMan qPCR was performed using custom TaqMan probe and primers specific for the bovine growth hormone polyadenylation (BGH poly(A)) sequences in the transgene cassette and compared with a standard curve (forward primer, 5′-CCTCGACTGTGCCTTCTAG-3′; reverse primer, 5′-TGCGATGCAATTTCCTCAT-3′; and probe, 5′-FAM-TGCCAGCCATCTGTTGTTTGCC-MGB). To ensure an equal genomic DNA input for each sample, a separate qPCR was performed to detect GAPDH genomic DNA, using TaqMan probe and primer sets (Thermo Fisher Scientific, assay IDMm 01180221_g1, gene symbol Gm12070). The AAV vector gc for each sample were normalized by considering any differences in GAPDH Ct (cycle threshold) values using the following formula: (AAV vector gc)/($2^{\Delta Ct}$). The ΔCt value was calculated as GAPDH Ct value (sample of interest) − average GAPDH Ct value (sample with highest Ct value). Data were expressed as AAV gc per 50 ng of genomic DNA.

Digital-Droplet PCR

The TaqMan PCR reaction mixture consists of ddPCR (Droplet Digital PCR)Supermix for Probes (No dUTP) (Bio-Rad catalog no.1863024), 20× primer, and probes and template (1 μL) in a final volume of 20 μL. Custom TaqMan probe and primers were used specific for the FLAG tag and merlin 3′ end of the transgene expression cassette (forward primer, 5′-GACTACAAGGACGATGACGATAAG-3′; reverse primer, 5′-TCTTGGGTTGCTTCCTCTTG-3′; probe, 5′-FAM- ATCGCTTCCCGCATGAGCTTCA-3′). Using the Automated Droplet Generator QX200 AutoDG Droplet Digital System from Bio-Rad (Hercules, CA), each assembled ddPCR reaction mixture was then loaded into the sample well of an eight-channel disposable droplet DG32 Cartridges for QX200 (catalog no. 1864108). A volume of 20 μL of droplet generation oil (Bio-Rad catalog no. 1864110) was loaded into the oil well for each channel. The plate was heat sealed with a foil seal and then placed on a conventional thermal cycler and amplified to the end point according to the manufacturer's cycling conditions. After PCR, the 96-well PCR plate was

loaded on the droplet reader (Bio-Rad) and analysis of the ddPCR data was performed with QuantaSoft analysis software (Bio-Rad).

DATA AND CODE AVAILABILITY

The data used to support the findings of this study are included within the article and the supplementary material.

SUPPLEMENTAL INFORMATION

Supplemental information can be found online at https://doi.org/10.1016/j.omtm.2022.06.012.

ACKNOWLEDGMENTS

We thank Ms. Suzanne McDavitt for skilled editorial assistance and Dr. Koen Breyne for advice with statistical calculations. Drs. Konstantina Stankovic, Lei Xu, Gary Brenner, Xuan Zhang, and Jessica Sagers (Massachusetts General Hospital) provided their early insights into this work. Dr. Miguel Sena-Esteves (UMass Medical Center) contributed the AAV backbone plasmid. We also thank Dr. Margaret Wallace (University of Florida) for providing immortalized human SCs. The authors gratefully acknowledge Cochava and Urri Rubin for their generous support of this project (S.P.). Other support included National Institutes of Health R01-DC017117 (C.A.M.), Cure Alzheimer's Fund Award (C.A.M.), National Institutes of Health R01 NS113854 (V.R.), and U19 CA179563 through the NIH Common Fund, the Office of Strategic Coordination/Office of the NIH Director (X.O.B.).

AUTHOR CONTRIBUTIONS

S.P., R.B., V.R., and X.O.B. wrote the manuscript. All authors edited the manuscript. S.P., C.A.M., R.B., V.R., S.R.P., D.B.W., K.M., and X.O.B. designed the experiments. S.P., R.B., P.S.C., G.M., A.Y., E.A.H., S.L., A.K., K.M., and E.H. performed the experiments. S.P., R.B., V.R., A.S.R., C.A.M., A.S.-R., and X.O.B. analyzed the data. C.A.M., V.R., and X.O.B. supervised the project.

DECLARATION OF INTERESTS

C.A.M. has a financial interest in Chameleon Biosciences, Inc. and Sphere Gene Therapeutics, companies developing an enveloped AAV vector platform technology. C.A.M. also has a financial interest in Skylark Bio, which is developing gene therapy to treat hereditary hearing loss. C.A.M.'s interests were reviewed and are managed by MGH and Partners HealthCare in accordance with their conflict of interest policies. D.B.W. is a consultant for Skylark Bio, Inc., Recursion Pharmaceuticals, Mulberry Biotherapeutics, and NF2 Biosolutions. The other authors declare no competing interests.

REFERENCES

1. Lu-Emerson, C., and Plotkin, S.R. (2009). The neurofibromatoses. Part 1: NF1. Rev. Neurol. Dis. *6*, E47–E53.

2. Petrilli, A.M., and Fernández-Valle, C. (2016). Role of Merlin/NF2 inactivation in tumor biology. Oncogene *35*, 537–548. https://doi.org/10.1038/onc.2015.125.

3. Stamenkovic, I., and Yu, Q. (2010). Merlin, a "magic" linker between extracellular cues and intracellular signaling pathways that regulate cell motility, proliferation, and survival. Curr. Protein Pept. Sci. *11*, 471–484.

4. James, M.F., Han, S., Polizzano, C., Plotkin, S.R., Manning, B.D., Stemmer-Rachamimov, A.O., Gusella, J.F., and Ramesh, V. (2009). NF2/merlin is a novel negative regulator of mTOR complex 1, and activation of mTORC1 is associated with meningioma and schwannoma growth. Mol. Cell Biol. *29*, 4250–4261. https://doi.org/10.1128/mcb.01581-08.

5. López-Lago, M.A., Okada, T., Murillo, M.M., Socci, N., and Giancotti, F.G. (2009). Loss of the tumor suppressor gene NF2, encoding merlin, constitutively activates integrin-dependent mTORC1 signaling. Mol. Cell Biol. *29*, 4235–4249.

6. James, M.F., Stivison, E., Beauchamp, R., Han, S., Li, H., Wallace, M.R., Gusella, J.F., Stemmer-Rachamimov, A.O., and Ramesh, V. (2012). Regulation of mTOR complex 2 signaling in neurofibromatosis 2-deficient target cell types. Mol. Cancer Res. *10*, 649–659. https://doi.org/10.1158/1541-7786.mcr-11-0425-t.

7. Beauchamp, R.L., James, M.F., DeSouza, P.A., Wagh, V., Zhao, W.N., Jordan, J.T., Stemmer-Rachamimov, A., Plotkin, S.R., Gusella, J.F., Haggarty, S.J., and Ramesh, V. (2015). A high-throughput kinome screen reveals serum/glucocorticoid-regulated kinase 1 as a therapeutic target for NF2-deficient meningiomas. Oncotarget *6*, 16981–16997.

8. McClatchey, A.I., and Fehon, R.G. (2009). Merlin and the ERM proteins–regulators of receptor distribution and signaling at the cell cortex. Trends Cell Biol. *19*, 198. https://doi.org/10.1016/j.tcb.2009.02.006.

9. Shaw, R.J., Paez, J.G., Curto, M., Yaktine, A., Pruitt, W.M., Saotome, I., O'Bryan, J.P., Gupta, V., Ratner, N., Der, C.J., et al. (2001). The Nf2 tumor suppressor, merlin, functions in Rac-dependent signaling. Dev. Cell *1*, 63–72.

10. Yi, C., Wilker, E.W., Yaffe, M.B., Stemmer-Rachamimov, A., and Kissil, J.L. (2008). Validation of the p21-activated kinases as targets for inhibition in neurofibromatosis type 2. Cancer Res. *68*, 7932–7937. https://doi.org/10.1158/0008-5472.can-08-0866.

11. Hamaratoglu, F., Willecke, M., Kango-Singh, M., Nolo, R., Hyun, E., Tao, C., Jafar-Nejad, H., and Halder, G. (2006). The tumour-suppressor genes NF2/Merlin and Expanded act through Hippo signalling to regulate cell proliferation and apoptosis. Nat. Cell Biol. *8*, 27–36.

12. Yin, F., Yu, J., Zheng, Y., Chen, Q., Zhang, N., and Pan, D. (2013). Spatial organization of Hippo signaling at the plasma membrane mediated by the tumor suppressor Merlin/NF2. Cell *154*, 1342–1355.

13. Li, W., You, L., Cooper, J., Schiavon, G., Pepe-Caprio, A., Zhou, L., Ishii, R., Giovannini, M., Hanemann, C.O., Long, S.B., et al. (2010). Merlin/NF2 suppresses tumorigenesis by inhibiting the E3 ubiquitin ligase CRL4(DCAF1) in the nucleus. Cell *140*, 477–490.

14. Scoles, D.R. (2008). The merlin interacting proteins reveal multiple targets for NF2 therapy. Biochim. Biophys. Acta *1785*, 32–54.

15. Hartmann, M., Parra, L.M., Ruschel, A., Böhme, S., Li, Y., Morrison, H., Herrlich, A., and Herrlich, P. (2015). Tumor suppressor NF2 blocks cellular migration by inhibiting ectodomain cleavage of CD44. Mol. Cancer Res. *13*, 879–890. https://doi.org/10.1158/1541-7786.mcr-15-0020-t.

16. Fernandez-Valle, C., Tang, Y., Ricard, J., Rodenas-Ruano, A., Taylor, A., Hackler, E., Biggerstaff, J., and Iacovelli, J. (2002). Paxillin binds schwannomin and regulates its density-dependent localization and effect on cell morphology. Nat. Genet. *31*, 354–362.

17. James, M.F., Manchanda, N., Gonzalez-Agosti, C., Hartwig, J.H., and Ramesh, V. (2001). The neurofibromatosis 2 protein product merlin selectively binds F-actin but not G-actin, and stabilizes the filaments through a lateral association. Biochem. J. *356*, 377–386. https://doi.org/10.1042/bj3560377.

18. Wiederhold, T., Lee, M.F., James, M., Neujahr, R., Smith, N., Murthy, A., Hartwig, J., Gusella, J.F., and Ramesh, V. (2004). Magicin, a novel cytoskeletal protein associates with the NF2 tumor suppressor merlin and Grb2. Oncogene *23*, 8815–8825.

19. Giovannini, M., Bonne, N.X., Vitte, J., Chareyre, F., Tanaka, K., Adams, R., Fisher, L.M., Valeyrie-Allanore, L., Wolkenstein, P., Goutagny, S., and Kalamarides, M. (2014). mTORC1 inhibition delays growth of neurofibromatosis type 2 schwannoma. Neuro Oncol. *16*, 493–504. https://doi.org/10.1093/neuonc/not242.

20. Sagers, J.E., Beauchamp, R.L., Zhang, Y., Vasilijic, S., Wu, L., DeSouza, P., Seist, R., Zhou, W., Xu, L., Ramesh, V., and Stankovic, K.M. (2020). Combination therapy with mTOR kinase inhibitor and dasatinib as a novel therapeutic strategy for vestibular schwannoma. Sci. Rep. *10*, 4211. https://doi.org/10.1038/s41598-020-60156-6.

21. Bai, Y., Liu, Y.J., Wang, H., Xu, Y., Stamenkovic, I., and Yu, Q. (2007). Inhibition of the hyaluronan-CD44 interaction by merlin contributes to the tumor-suppressor activity of merlin. Oncogene *26*, 836–850.

22. Chiasson-MacKenzie, C., Morris, Z.S., Liu, C.H., Bradford, W.B., Koorman, T., and McClatchey, A.I. (2018). Merlin/ERM proteins regulate growth factor-induced macropinocytosis and receptor recycling by organizing the plasma membrane:cytoskeleton interface. Genes Dev. *32*, 1201–1214.

23. Plotkin, S.R., Merker, V.L., Halpin, C., Jennings, D., McKenna, M.J., Harris, G.J., and Barker, F.G. (2012). Bevacizumab for progressive vestibular schwannoma in neurofibromatosis type 2: a retrospective review of 31 patients. Otol. Neurotol. *33*, 1046–1052. https://doi.org/10.1097/mao.0b013e31825e73f5.

24. Slusarz, K.M., Merker, V.L., Muzikansky, A., Francis, S.A., and Plotkin, S.R. (2014). Long-term toxicity of bevacizumab therapy in neurofibromatosis 2 patients. Cancer Chemother. Pharmacol. *73*, 1197–1204. https://doi.org/10.1007/s00280-014-2456-2.

25. Williams, D.A., and Thrasher, A.J. (2014). Concise review: lessons learned from clinical trials of gene therapy in monogenic immunodeficiency diseases. Stem Cells Transl. Med. *3*, 636–642. https://doi.org/10.5966/sctm.2013-0206.

26. High, K.A., and Anguela, X.M. (2016). Adeno-associated viral vectors for the treatment of hemophilia. Hum. Mol. Genet. *25*, R36–R41. https://doi.org/10.1093/hmg/ddv475.

27. Day, J.W., Finkel, R.S., Chiriboga, C.A., Connolly, A.M., Crawford, T.O., Darras, B.T., Iannaccone, S.T., Kuntz, N.L., Peña, L.D.M., Shieh, P.B., et al. (2021). Onasemnogene abeparvovec gene therapy for symptomatic infantile-onset spinal muscular atrophy in patients with two copies of SMN2 (STR1VE): an open-label, single-arm, multicentre, phase 3 trial. Lancet Neurol. *20*, 284–293.

28. Pierce, E.A., and Bennett, J. (2015). The status of RPE65 gene therapy trials: safety and efficacy. Cold Spring Harb. Perspect. Med. *5*, a017285. https://doi.org/10.1101/cshperspect.a017285.

29. Mendell, J.R., Al-Zaidy, S.A., Rodino-Klapac, L.R., Goodspeed, K., Gray, S.J., Kay, C.N., Boye, S.L., Boye, S.E., George, L.A., Salabarria, S., et al. (2021). Current clinical applications of in vivo gene therapy with AAVs. Mol. Ther. *29*, 464–488.

30. Prabhakar, S., Taherian, M., Gianni, D., Conlon, T.J., Fulci, G., Brockmann, J., Stemmer-Rachamimov, A.O., Sena-Esteves, M., Breakefield, X.O., and Brenner, G.J. (2013). Regression of schwannomas induced by adeno-associated virus-mediated delivery of caspase-1. Hum. Gene Ther. *24*, 152–162. https://doi.org/10.1089/hum.2012.094.

31. Hall, J., Prabhakar, S., Balaj, L., Lai, C.P., Cerione, R.A., and Breakefield, X.O. (2016). Delivery of therapeutic proteins via extracellular vesicles: review and potential treatments for Parkinson's disease, glioma and schwannoma. Cell. Mol. Neurobiol. *36*, 417–427. https://doi.org/10.1007/s10571-015-0309-0.

32. Ahmed, S.G., Abdelanabi, A., Doha, M., and Brenner, G.J. (2019). Schwannoma gene therapy by adeno-associated virus delivery of the pore-forming protein Gasdermin-D. Cancer Gene Ther. *26*, 259.

33. Ahmed, S.G., Abdelnabi, A., Maguire, C.A., Doha, M., Sagers, J.E., Lewis, R.M., Muzikansky, A., Giovannini, M., Stemmer-Rachamimov, A., Stankovic, K.M., et al. (2019). Gene therapy with apoptosis-associated speck-like protein, a newly described schwannoma tumor suppressor, inhibits schwannoma growth in vivo. Neuro Oncol. *21*, 854–866.

34. Ahmed, S.G., Hadaegh, F., and Brenner, G.J. (2019). Developing myelin specific promoters for schwannoma gene therapy. J. Neurosci. Methods *323*, 77–81. https://doi.org/10.1016/j.jneumeth.2019.05.007.

35. György, B., Fitzpatrick, Z., Crommentuijn, M.H., Mu, D., and Maguire, C.A. (2014). Naturally enveloped AAV vectors for shielding neutralizing antibodies and robust gene delivery in vivo. Biomaterials *35*, 7598–7609. https://doi.org/10.1016/j.biomaterials.2014.05.032.

36. Saydam, O., Ozdener, G.B., Senol, O., Mizrak, A., Prabhakar, S., Stemmer-Rachamimov, A.O., Breakefield, X.O., and Brenner, G.J. (2011). A novel imaging-compatible sciatic nerve schwannoma model. J. Neurosci. Methods *195*, 75–77. https://doi.org/10.1016/j.jneumeth.2010.10.021.

37. Ahmad, I., Fernando, A., Gurgel, R., Jason Clark, J., Xu, L., and Hansen, M.R. (2015). Merlin status regulates p75(NTR) expression and apoptotic signaling in Schwann cells following nerve injury. Neurobiol. Dis. *82*, 114–122. https://doi.org/10.1016/j.nbd.2015.05.021.

38. Mizrak, A., Bolukbasi, M.F., Ozdener, G.B., Brenner, G.J., Madlener, S., Erkan, E.P., Ströbel, T., Breakefield, X.O., and Saydam, O. (2013). Genetically engineered microvesicles carrying suicide mRNA/protein inhibit schwannoma tumor growth. Mol. Ther. *21*, 101–108. https://doi.org/10.1038/mt.2012.161.

39. Gehlhausen, J.R., Park, S.J., Hickox, A.E., Shew, M., Staser, K., Rhodes, S.D., Menon, K., Lajiness, J.D., Mwanthi, M., Yang, X., et al. (2015). A murine model of neurofibromatosis type 2 that accurately phenocopies human schwannoma formation. Hum. Mol. Genet. *24*, 1–8. https://doi.org/10.1093/hmg/ddu414.

40. Bonne, N.X., Vitte, J., Chareyre, F., Karapetyan, G., Khankaldyyan, V., Tanaka, K., Moats, R.A., and Giovannini, M.J. (2016). An allograft mouse model for the study of hearing loss secondary to vestibular schwannoma growth. Neuro Oncol. *129*, 47–56. https://doi.org/10.1007/s11060-016-2150-9.

41. Chen, J., Landegger, L.D., Sun, Y., Ren, J., Maimon, N., Wu, L., Ng, M.R., Chen, J.W., Zhang, N., Zhao, Y., et al. (2019). A cerebellopontine angle mouse model for the investigation of tumor biology, hearing, and neurological function in NF2-related vestibular schwannoma. Nat. Protoc. *14*, 541–555. https://doi.org/10.1038/s41596-018-0105-7.

42. Boetto, J., Peyre, M., and Kalamarides, M. (2021). Mouse models in meningioma research: a systematic review. Cancers *13*, 3712. https://doi.org/10.3390/cancers13153712.

43. Andradas, C., Byrne, J., Kuchibhotla, M., Ancliffe, M., Jones, A.C., Carline, B., Hii, H., Truong, A., Storer, L.C.D., Ritzmann, T.A., et al. (2021). Assessment of cannabidiol and Δ9-Tetrahydrocannabiol in mouse models of medulloblastoma and ependymoma. Cancers *13*, 330. https://doi.org/10.3390/cancers13020330.

44. Li, H., Chang, L.J., Neubauer, D.R., Muir, D.F., and Wallace, M.R. (2016). Immortalization of human normal and NF1 neurofibroma Schwann cells. Lab. Invest. *96*, 1105–1115. https://doi.org/10.1038/labinvest.2016.88.

45. Prabhakar, S., Brenner, G.J., Sung, B., Mao, J., Sena-Esteves, M., Stemmer-Rachamimov, A., Tannous, B., Breakefield, X.O., and Stemmer-RAchAmimov, A. (2010). Imaging and therapy of experimental schwannomas using HSV amplicon vector-encoding apoptotic protein under Schwann cell promoter. Cancer Gene Ther. *17*, 266–274. https://doi.org/10.1038/cgt.2009.71.

46. Giovannini, M., Robanus-Maandag, E., van der Valk, M., Niwa-Kawakita, M., Abramowski, V., Goutebroze, L., Woodruff, J.M., Berns, A., and Thomas, G. (2000). Conditional biallelic Nf2 mutation in the mouse promotes manifestations of human neurofibromatosis type 2. Genes Dev. *14*, 1617–1630. https://doi.org/10.1101/gad.14.13.1617.

47. Ivanchenko, M.V., Hanlon, K.S., Devine, M.K., Tenneson, K., Emond, F., Lafond, J.F., Kenna, M.A., Corey, D.P., and Maguire, C.A. (2020). Preclinical testing of AAV9-PHP.B for transgene expression in the non-human primate cochlea. Hear. Res. *394*, 107930. https://doi.org/10.1016/j.heares.2020.107930.

48. Meliani, A., Boisgerault, F., Fitzpatrick, Z., Marmier, S., Leborgne, C., Collaud, F., Simon Sola, M., Charles, S., Ronzitti, G., Vignaud, A., et al. (2017). Enhanced liver gene transfer and evasion of preexisting humoral immunity with exosome-enveloped AAV vectors. Blood Adv. *1*, 2019–2031. https://doi.org/10.1182/bloodadvances.2017010181.

49. Volak, A., LeRoy, S.G., Natasan, J.S., Park, D.J., Cheah, P.S., Maus, A., Fitzpatrick, Z., Hudry, E., Pinkham, K., Gandhi, S., et al. (2018). Virus vector-mediated genetic modification of brain tumor stromal cells after intravenous delivery. J. Neuro Oncol. *139*, 293–305. https://doi.org/10.1007/s11060-018-2889-2.

50. Xu, L., Gonzalez-Agosti, C., Beauchamp, R., Pinney, D., Sterner, C., and Ramesh, V. (1998). Analysis of molecular domains of epitope-tagged merlin isoforms in Cos-7 cells and primary rat Schwann cells. Exp. Cell Res. *238*, 231–240. https://doi.org/10.1006/excr.1997.3843.

51. Schindelin, J., Arganda-Carreras, I., Frise, E., Kaynig, V., Longair, M., Pietzsch, T., Preibisch, S., Rueden, C., Saalfeld, S., Schmid, B., et al. (2012). Fiji: an open-source platform for biological-image analysis. Nat. Methods *9*, 676–682. https://doi.org/10.1038/nmeth.2019.